A Winding Function-Based Model of Air-gap Eccentricity in Saturated Induction Motors

A. Ghoggal, S.E. Zouzou, M. Sahraoui, H. Derghal and A. Hadri-Hamida.

Abstract — **This paper set out a new modeling technique of air-gap eccentricity in induction motors (IMs) taking into account teeth saturation due to the local air-gap flux concentration. The approach is based on the inclusion of the magnetic saturation into the analytical model by a fictive permeance variation. Besides that, it supposes that, in air-gap nonuniformity conditions, the well-known saturation factor must be updated in function of the spatial-dependant air-gap length. The 2D-modified winding function approach (2D-MWFA) is utilized to get the inductance formalism while assuming a linear rise of the saturation factor with respect to the air-gap length in a particular circumferential region. We show that the proposed model yields more reasonable results by confirming that the magnetic saturation effect reduces the asymmetry of the air-gap flux distribution due to the eccentricity. Furthermore, we highlight this effect by inspecting the shapes of the calculated inductances and making them ready for a full dynamic simulation in sense of multiple coupled circuit model (MCCM).**

Index Terms — **Induction motor, 2D-MWFA, convolution, FFT, Diagnosis, space harmonics, skew, teeth saturation, static eccentricity.**

I. Introduction

SINCE the nineties, winding function approach (WFA)-based modeling of electric machines attracts a growing number of researchers and students with a special emphasis on faults diagnosis. Although all its recognized versions assume until now a radial air-gap field and an infinite permeability of iron, which means that the air-gap is the main zone of electromagnetic interactions, they have proved to be convenient in predicting the behaviors of some common fault indexes. Compared to the relevant finite elements method (FEM), MWFA exploits advantageously the air-gap permeance distortions and yields fast results by involving only few constructional parameters. However, some criticisms concerning its accuracy and aptitude to deal with some practical cases and that in comparison with the FEM and the flux models have been mentioned recently [1],[2].

The slot permeance effect and the nonlinearity of the magnetic material are among the major sources of disagreement between the results of the FEM and those obtained from WFA. In [3], Nandi proposed a model that takes into account the permeance of the stator and rotor slots by involving the MWFA and the MCCM [4]. Besides that, he discussed slotting effects on the spectral content of the line current. While Ilamparithi *et al.* found in [5] that close results held through linear and nonlinear model (MWFA and FEM), Faiz *et al.* in [1] state that, with an eccentric rotor, the classical MWFA-based model yields a large magnetic field amplitude and further irregularities of the air-gap flux density compared to the FEM and the experimental measurements. This fact gave way to an overestimation of the amplitudes of the fault related harmonics. Furthermore, one can find in reference [2] other convincing arguments proving the necessity of saturation modeling. This was the aim of [6] where the author shows that the saturation can also be included into the MCCM and MWFA-based model thanks to a fictive air-gap variation [7]. In its first version, this model handles the case of healthy IM. For the first time, Faiz *et al.* in [8] enlarge the scope of the MWFA by exploring the stator inductance fluctuations due to the saturation of the main magnetic flux path in case of eccentricity. The total inverse of the air-gap function involves components related to both saturation and eccentricity such as

$$g^{-1} = g_0^{-1} \cdot g_{sat}^{-1} \cdot g_{ecc}^{-1} \tag{1}$$

- g_0 is the geometrical air-gap length in symmetrical conditions.
- g_{sat} is the saturation related part of the air-gap function to insure the flattened form of the flux density. It is calculated in reference to a fixed saturation factor for a chosen operational mode.
- g_{ecc} is the air-gap function part due to the eccentricity.

It is important to note that defining g_{sat}^{-1} in (1) without taking into account the varying air-gap length may indicate that the level of saturation depends only on the magnetic field position. In order to reach better results, we present here a new 2D-MWFA-based model of saturation in IM by investigating the fact that, in air-gap eccentricity conditions, the saturation factor is a function of the air-gap field position as well as the air-gap length. The study is supported by the estimation of the flux density shapes and the profiles of the derived inductances.

II. Modeling of Eccentricity in Saturated IM

A. Preamble

By admitting that teeth saturation is most significant than corps saturation in operational IMs, the saturation can be integrated into the analytical model by assuming a suitable decrease of the air-gap permeance with respect to the magnitude and position of the main air-gap flux [7]. Even in symmetrical conditions, the saturation level is primarily related to many factors such as the supply voltage. It compares the air-gap flux density to that corresponding to

This work was supported by the Electrical Engineering Department, Mentouri University, the LEC laboratory - Constantine and the LGEB laboratory - Med Khider University - 07000 Biskra - Algeria.

A. Ghoggal , M. Sahraoui and A. Hadri-Hamida are with Mentouri University – Constantine - Algeria (e-mail: ghoetudes@yahoo.fr, s_moh78@yahoo.fr).

S.E. Zouzou and H. Derghal are with "Laboratoire de Génie Electrique de Biskra" (LGEB), Med Khider University - 07000 Biskra - Algeria (e-mail: zouzou_s@Hotmail.com)

978-1-4673-0141-1/12/$26.00 ©2012 IEEE

the linear magnetic characteristic in a specified state. This leads to the known saturation factor which is indeed a ratio able to limit the permeance to a value matching the actual air-gap flux density. Therefore, this factor must increase or decreases when the permeance itself varies as a consequence of a rotor eccentricity. As reported by Ossama *et al.* in [9], *the air-gap nonuniformity imposes that the saturation level must vary along the machine periphery with respect to the flux density value. Accordingly higher saturation occurs at the narrow air-gap than at the large one.* This implies that the reluctance increases considerably at the smaller air-gap [10], but it is slightly affected by saturation, as far as we even reach the linear magnetic characteristic, at the larger one. In the light of this point of view, the saturation factor must be adjusted with respect to the air-gap length. In other words, we can admit in an extended IM model including both saturation and eccentricity that, if at an angular position the air-gap length is equal to that of the symmetric machine, the fictive air-gap length is obtained from the common expression given in [7] whereas the saturation factor is identified from the ratio of the fundamental components of the air-gap voltage of the saturated and unsaturated symmetric IM. For any other angular position, the saturation parameters must be revaluated in order to reflect the local level of the flux density tolerated by the iron region.

B. The inverse of the air-gap function

The reader can find in [11] one of the methods that deals with the modeling of air-gap eccentricity and the calculation of IM inductances starting originally from the 2D-MWFA. It should be noted that, thanks to numerical convolution algorithms, there is generally no need for Fourier series expansion neither for the inverse of air-gap function nor for the turn functions whatever their level of complexity. However, this technique is not yet adapted to all the known cases. To expose the suggested approach, we distinguish here effective quantities when the saturation is excluded and fictive ones when we involve the model of teeth saturation. In symmetrical conditions, the fictive inverse of air-gap function is [7]

$$g^{-1}(\varphi,\theta_f) = K_e + K_m \cos\{2(p.\varphi - \theta_f)\} \qquad (2)$$

with:

$$K_m = \frac{2\cdot\{K_s - 1\}}{3\cdot K_s} g_0^{-1} \qquad (3)$$

$$K_e = \frac{K_s + 2}{3\cdot K_s} g_0^{-1} \qquad (4)$$

K_s is the saturation factor in symmetrical condition, p is the pole pair number, φ is a geometric angle measured with respect to a fixed stator reference and the electric angle θ_f is the position of the air-gap magnetic field as described in [7]. As a simple choice of expressing equations and formulas in accordance with the plan representation introduced in [11] which was the base of adapting the convolution based technique in the calculation of the inductances [12], we take for any arc of circumference x in meter the corresponding arc in radian $\hat{x} = x/r_0$. Now, following the above explanation, the inverse of air-gap function in an eccentricity condition can be written as

$$g_{ecc}^{-1}(x, x_f, x_r) = \acute{K}_e(\acute{g}_0) + \acute{K}_m(\acute{g}_0)\cdot\cos\{2(p.\hat{x} - \hat{x}_f)\} \qquad (5)$$

with $x = \varphi.r_0$, $x_f = \theta_f.r_0$ and $x_r = \theta_r.r_0$. Angle θ_r is the rotor position. As for $\acute{K}_e$ and $\acute{K}_m$, they are given by:

$$\acute{K}_m(\acute{g}_0) = \frac{2\cdot\{K(\acute{g}_0) - 1\}}{3\cdot K(\acute{g}_0)} \acute{g}_0^{-1}(x, x_r) \qquad (6)$$

$$\acute{K}_e(\acute{g}_0) = \frac{K(\acute{g}_0) + 2}{3\cdot K(\acute{g}_0)} \acute{g}_0^{-1}(x, x_r) \qquad (7)$$

with

$$\acute{g}_0^{-1}(x, x_r) = \frac{1}{g_0\{1 - \delta_s\cdot\cos(\hat{x}) - \delta_d.\cos(\hat{x} - \hat{x}_r)\}} \qquad (8)$$

The minimum effective air-gap is taken at $\hat{x} = 0$. Equations (5)-(7) signify that $\acute{K}_m$, $\acute{K}_e$ as well as the adjusted or local saturation factor K depend on the effective air-gap length $\acute{g}_0$ which, under air-gap eccentricity conditions, depends on g_0, x and x_r. Fig. 1 depicts an evolution curve of the saturation factor with respect to $\acute{g}_0$. As can be seen, K is delimited by K_{max} and 1 while passing through K_s when the air-gap becomes equal to that of the symmetric machine. K_{max} denotes the saturation factor at the minimum effective air-gap $\acute{g}_{0min}$. One can already write

$$K(\acute{g}_0) = K_s \quad \text{if} \quad \acute{g}_0(x) = g_0 \qquad (9)$$

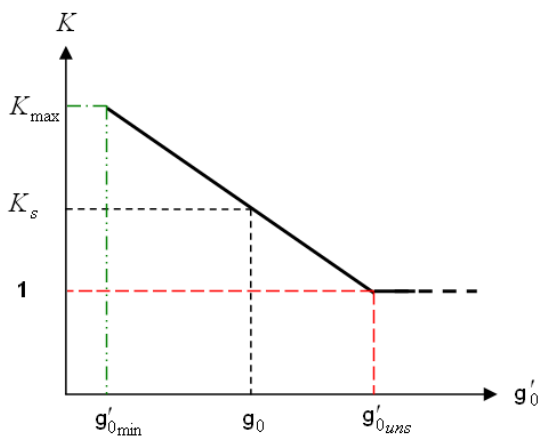

Fig. 1. Evolution model of the adjusted saturation factor as a function of the effective air-gap length in case of eccentricity.

According to (2), the biggest value of the fictive air-gap function, which goes with the maximum of the flux density curve in a specified condition, can be easily estimated. By a reverse reasoning, we can admit that at the position where the effective air-gap length in an eccentricity case reaches that value, called $\acute{g}_{0uns}$, no more saturation can occur. This is translated as

$$K(\acute{g}_0) = 1 \quad \text{if} \quad \acute{g}_0(x) \geq \acute{g}_{0uns} \qquad (10)$$

and from (2) we get

$$\acute{g}_{0uns} = 1/(K_e - K_m) \tag{11}$$

As shown in fig. 1, we assume first a linear rise of the adjusted saturation factor K between these two points: (g_0, K_s) and $(\acute{g}_{0uns}, 1)$. So

$$K(\acute{g}_0) = A.\acute{g}_0(x) + C \tag{12}$$

Relations (9)-(12) yield

$$\begin{cases} A = \left(\frac{1}{4}K_s - 1\right) \cdot g_0^{-1} \\ C = \frac{3}{4}K_s + 1 \end{cases} \tag{13}$$

(5)-(8) and (12)-(13) describe completely the suggested model of the fictive inverse of the air-gap function when the air-gap varies as a consequence of a rotor eccentricity.

C. Static eccentricity modeling

The inverse of the air-gap function in case of static eccentricity is taken from (8) while considering $\delta_d = 0$. Even though pure static eccentricity can be modeled mathematically, it was shown in previous work that, due the ensuing unbalanced magnetic poles, an amount of dynamic eccentricity occurs in practice leading to a mixed eccentricity form. We begin with a pure static eccentricity case by illustrating plots of $K(\varphi)$ and $K(\acute{g}_0)$ related to a 3kW, 2-pole, 3-phase stator winding. The motor has 36 stator slots and 28 skewed rotor bars (fig. 2). It can be seen that the local saturation factor at the narrowest air-gap for 40% of static eccentricity reaches a big value over that of what can be expected for a typical symmetrical machine [6].

Equations (8) and (12) yield

$$K_{max} = K_s + \delta_s(1 - 0.25K_s) \tag{14}$$

Taking $\delta_s = 0.4$ and $K_s = 1.1$ yields $K_{max} = 1.39$. For $\hat{x}_{uns} \leq \hat{x} \leq 2\pi - \hat{x}_{uns}$, there is no saturation. The substitution of (8) in (11) leads to

$$\hat{x}_{uns} = \varphi_{uns} = \cos^{-1}\left(\frac{g_0 - K_e + K_m}{\delta_s . g_0}\right) \tag{15}$$

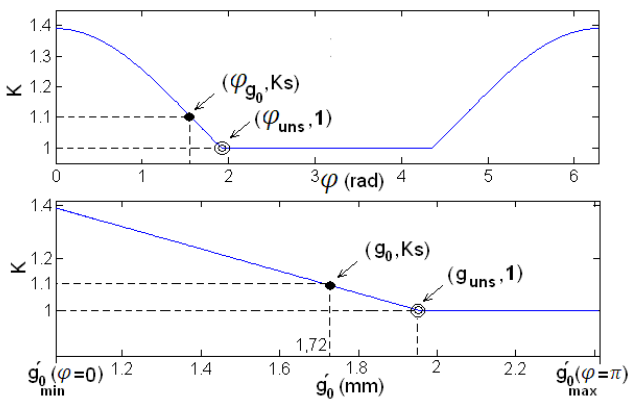

Fig. 2. Evolution of the adjusted saturation factor K in function of the stator angle (top) and the effective air-gap (bottom) in case of 40% of static eccentricity ($K_s = 1.1$).

The fictive inverse of the air-gap function enclosing saturation and static eccentricity effects have to be lower than the equivalent effective quantity principally at and around the minimum air-gap, in particular when the position of the flux density maximum reaches that of the minimum air-gap. Fig. 3 illustrates an idealized flux density shape by considering that the position of its maximum coincides with the minimum effective air-gap ($\theta_f = -\frac{\pi}{2}$). Excluding saturation means that the effective inverse of air-gap function takes its highest values at that position. The other cases allow us to consider that teeth saturation reduces the permeance value with proportions specified by the adjusted saturation factor. That can be seen through the examination of the curve of the fictive inverse of the air-gap function which looks lower than that of the unsaturated case but approaches it when moving away from the position of the minimum effective air-gap.

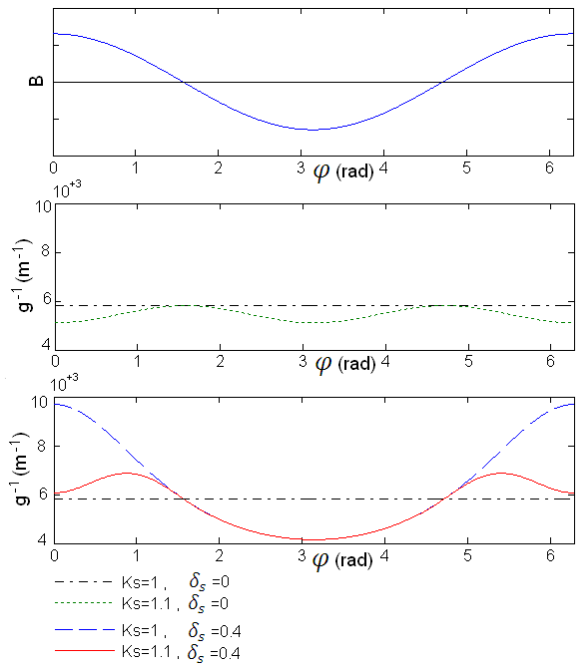

Fig. 3. A typical shape of the fundamental of the flux density (top), the inverse of air-gap function under uniform air-gap (middle) and that related to static eccentricity (bottom) all for p=1 and $\theta_f = -\pi/2$.

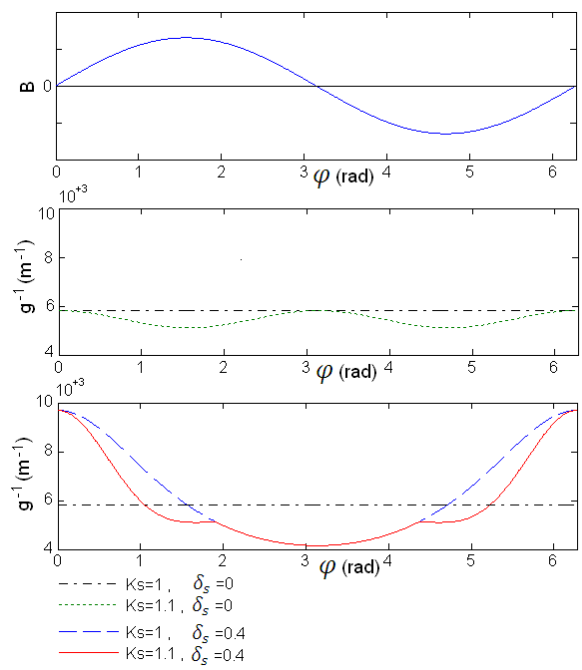

Fig. 4. A typical shape of the fundamental of the flux density (top), the inverse of air-gap function under uniform air-gap (middle) and that related to static eccentricity (bottom) all for p=1 and $\theta_f = 0$.

In fig. 4 related to $\theta_f = \hat{x}_f = 0$, the fictive inverse of the air-gap function takes the same value as the effective one at $\hat{x} = 0$ because B is null at that position. Elsewhere, the ratio $g_{ecc(x)}^{-1}/\acute{g}_0^{-1}(x)$ is lower because of the relatively lower value of the ratio $\acute{g}_0^{-1}(x)/B(x)$ compared to the first case.

D. Prediction of the flux density shapes

In the spirit of the modeling of teeth saturation by the equivalent permeance variation and for an illustrative purpose, we suppose only in this section that the magneto motive force (MMF) is unaltered by the saturation and that only the fundamental air-gap MMF is responsible for the saturation harmonics. This assumption is similar to what was considered in [2] and [10]. This means that the saturation effect on the flux density shape comes only from the introduced fictive permeance variation. Later, in the iterative process (i.e. when solving the system of state variables of the MCCM), some saturation harmonics in the MMF might appear. Accordingly, one can admit that

$$B_{sat} \approx \mu_0 g^{-1}.F \tag{16}$$

where F denotes the fundamental component of the MMF and $g^{-1}$is taken from (2). This consideration should result in a flattened form of the flux density plot. In case of eccentricity, we can get a typical shape of the flux density from that of F by substituting the fictive inverse of the air-gap function in (16) by the corresponding one described by (5) for saturation and static eccentricity state. Hence

$$B_{sat+ecc} \approx \mu_0 g_{ecc}^{-1}.F \tag{17}$$

As shown in fig. 5 and fig. 6, the flux density is distributed along the air-gap with a more regular form compared to the case when the saturation is excluded. This is most evident in fig. 6 and the bottom of fig. 5 related to a moment when the maximum flux density coincides with the minimum effective air-gap. Note that at $\varphi = 0$, the saturation action on the flux density is most important implying a main effect on its relative plot.

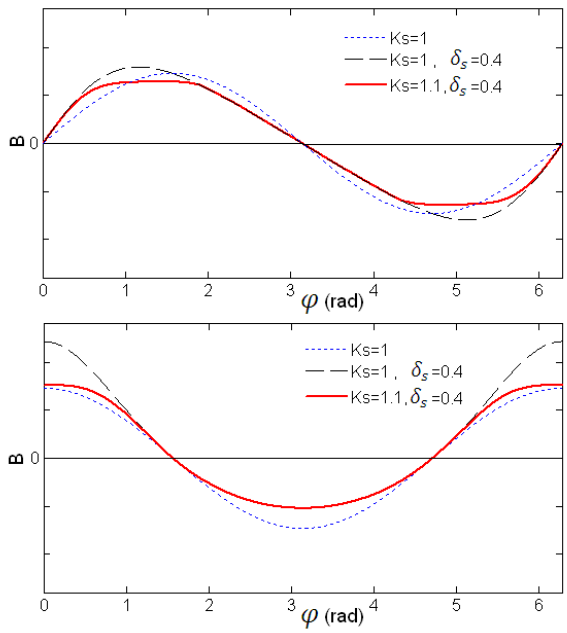

Fig. 5. Typical air-gap flux density wave forms for the cases: with and without eccentricity, and by including and excluding saturation. $\theta_f = 0$ (top) and $\theta_f = -\pi/2$ (bottom). p=1.

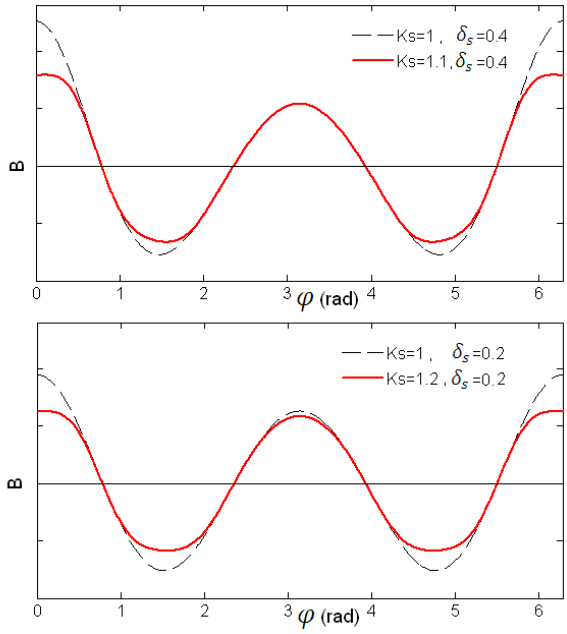

Fig. 6. Typical air-gap flux density wave forms of the eccentric IM when including and when excluding saturation. $\delta_s = 0.4$ (top) and $\delta_s = 0.2$ (bottom). $\theta_f = -\pi/2$. We suppose here that p=2.

E. Calculation of the stator-rotor mutual inductance

The skew of the rotor bars, the linear rise of the MMF across the slot, the space harmonics, teeth saturation and static eccentricity can now be included into the 2D-MWFA-based model [11]. However, reference [2] states that slot permeance effect could not affect the spectral content of the motor current. For this reason and in order to simplify the study, this effect is not accounted for by the present model. Starting from the usual expression of magnetizing winding inductances and mutual inductances, we can get the IM inductances related to the static radial eccentricity problem by allowing teeth saturation to be taken into account. We consider here the winding inductances related to the MCCM and we begin with the expression of the mutual inductance L_{Ar_j}between the stator phase A and the jth rotor loop while involving the fictive inverse of the air-gap function. According to fig. 7, L_{Ar_j} can be written as [12]

$$L_{Ar_j}(x_r, x_f) = \mu_0 \int_0^{2\pi r_0} \int_0^{l} N_A(x, x_f).\, g_{ecc}^{-1}(x, x_f).\, n_{rj}(x, z, x_r)\, .\, dzdx \tag{18}$$

with

$$N_A(x, x_f) = n_A(x) - \frac{\langle g^{-1}.n_A \rangle}{\langle g^{-1} \rangle} \tag{19}$$

$$n_A(x) = \sum_{i=0}^{v} n_{A_i}(x) \tag{20}$$

μ_0 is the permeability of the free space, N_A and n_A are the winding function and turns function of stator phase A respectively, A_i is the ith coil of phase A and n_{rj} is the jth rotor loop turn function. Knowing that

$$n_{rj}(x, z, x_r) = \begin{cases} 1, & x_{1j} < x < x_{2j}\,, z_{1j} < z < z_{2j} \\ 0, & Otherwise \end{cases} \tag{21}$$

(18) can be rewritten as

$$L_{Ar_j}(x_r,x_f) = \mu_0 \int_0^{2\pi r_0} N_A(x,x_f).g_{ecc}^{-1}(x,x_f).1.\{z_{2j}(x,x_r) - z_{1j}(x,x_r)\}.dx \quad (22)$$

with

$$z_{2j}(x,x_r) - z_{1j}(x,x_r) = 0 \;\; for\; x \geq x_{2j} \vee x \leq x_{1j} \quad (23)$$

$$z_{1j}(x,x_r) = \begin{cases} 0, & x_{1j} \leq x \leq (x_{1j} + r_0.\lambda_r) \\ \dfrac{l}{r_0\gamma}(x - x_r - j.\lambda_r r_0), & (x_{1j} + r_0.\lambda_r) \leq x \leq x_{2j} \end{cases} \quad (24)$$

$$z_{2j}(x,x_r) = \begin{cases} \dfrac{l}{r_0\gamma}(x - x_r - (j-1).\lambda_r r_0), & x_{1j} \leq x \leq (x_{1j} + r_0.\gamma) \\ l, & (x_{1j} + r_0.\gamma) \leq x \leq x_{2j} \end{cases} \quad (25)$$

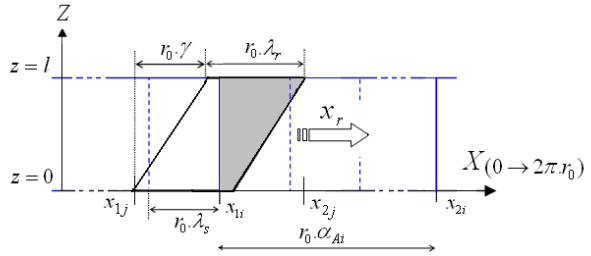

Fig. 7. Plane representation of the crossing of a skewed rotor loop under the field of the stator coils.

where $\lambda_r=2\pi/N_b$ is the rotor slot pitch, N_b the number of the rotor bars, α_{Ai} the stator coil pitch, γ the skew angle and (x_{1i}, x_{2i}) are the coordinates of the ends of the stator coil A_i. The rotor loop ends, (x_{1j}, x_{2j}), are defined by considering that x_r is measured with respect to the first end of the first rotor loop such as

$$\begin{cases} x_{1j} = x_r + (j-1).\lambda_r.r_0 \quad (i.e.\;\; x_{11} = x_r) \\ x_{2j} = x_r + (j.\lambda_r + \gamma).r_0 \end{cases} \quad (26)$$

For the particular case of static eccentricity, it is important to see that, even with the suggested additions to the initial saturation model, the inverse of the air-gap function described by (5) remains independent from x_r. Furthermore, it is shown in [12] that the integral bounds in the axial direction, (z_{1j}, z_{2j}), may be viewed as a function of one variable $(x_r - x)$ describing a shift instead of the double variable (x_r, x). It means that the convolution theorem can be once more a prerogative in order to carry out the inductance calculation task. Besides that, we should bear in mind that the convenience of this theorem in the actual purpose compared to the uniform air-gap situation is striking. In the symmetric case, one can prove the possibility of obtaining analytical expression of the inductance starting from its integral form, whereas in the actual case of static air-gap eccentricity it is not evident. Accordingly, convolution based solution appears here to be more than a choice. Note that in order to apply the convolution based technique, we seek to define all the rotor position functions using the dummy variable $\xi = (x_r - x)$. So taking

$$h(\xi) = z_{2j}(\xi) - z_{1j}(\xi) \quad (27)$$

(22) can be written as

$$L_{Ar_j}(x_r,x_f) = \mu_0 \int_0^{2\pi r_0} \underbrace{N_A(x,x_f).g_{ecc}^{-1}(x,x_f)}_{f_{x_f}(x)}.h(\xi).dx \quad (28)$$

Using (23), (24) and (25) yields

$$h(\xi) = \begin{cases} \dfrac{-l.(\xi + (j-1).\lambda_r r_0)}{r_0\gamma}, & \{(1-j).\lambda_r - \gamma\}.r_0 \leq \xi \leq (1-j).\lambda_r r_0 \\ l, & -j.\lambda_r.r_0 \leq \xi \leq \{(1-j).\lambda_r - \gamma\}.r_0 \\ l.\left(1 + \dfrac{1}{r_0\gamma}(\xi + j.\lambda_r.r_0)\right), & -(j.\lambda_r + \gamma).r_0 \leq \xi \leq -j.\lambda_r.r_0 \\ 0, & Otherwise \end{cases} \quad (29)$$

Now, a cyclic convolution form holds

$$L_{Ar_j}(x_r,x_f) = \mu_0 \left(f_{x_f} * h\right)(x_r) \quad (30)$$

A discrete form of (30) results from the division of an interval of size $2.\pi.r_0$ into m sampled values at equal intervals. The vector corresponding to the inductance values with respect to the rotor position corresponds to the m appropriate values resulting from the discrete convolution so as

$$\left(L_{Ar_j}\right)_m = \Delta.\mu_0.f_{x_f} * h \quad (31)$$

with

$$\Delta = 2\pi r_0/m \quad (32)$$

Many computer codes use convolution theorem to build convolution-based subroutines. For instance, the use of MATLAB function 'conv' is enough is such a case.

F. Calculation of the rotor inductances

The same analysis yields all the rotor inductances such as:

$$L_{mrj}(x_r,x_f) = 2\pi r_0 l\mu_0.\left(\langle g_{ecc}^{-1}.n_{rj}\rangle - \frac{\langle g_{ecc}^{-1}.n_{rj}\rangle^2}{\langle g_{ecc}^{-1}\rangle}\right) \quad (33)$$

$$L_{r_k rj}(x_r,x_f) = 2\pi r_0 l\mu_0.\left(-\frac{\langle g_{ecc}^{-1}.n_{rj}\rangle \cdot \langle g_{ecc}^{-1}.n_{rk}\rangle}{\langle g_{ecc}^{-1}\rangle}\right) \quad (34)$$

with $k \neq j$ and

$$\langle g_{ecc}^{-1}.n_{rj}\rangle = \frac{1}{2\pi r_0 l}\int_0^{2\pi r_0} \underbrace{g_{ecc}^{-1}(x,x_f)}_{f_{x_f}(x)}.h(x_r - x).dx \quad (35)$$

As $\langle g_{ecc}^{-1}\rangle$ do not depend on the rotor position, it is calculated only once for each magnetic field position using a simple numerical technique.

G. Calculation of the stator inductances

Practically, since stator magnetizing inductances do not vary with respect to x_r, there is no need to use convolution-based technique or to search analytical expressions of the stator magnetizing inductances. Accordingly, for any value of x_f, the stator inductances can be calculated only once using a classical numerical technique.

III. Numerical Results

The described technique was applied to the same 2-pole IM as previously. Fig. 8 to fig. 11 depict the curves of the calculated stator and rotor inductances and their first derivatives with respect to the rotor and air-gap field positions. Clearly, the added part of the permeance function due to saturation can be seen to affect the shapes of the inductances and their derivatives. We take similar observations as regards the rotor-stator mutual inductance and its derivatives (fig. 12 to 14). The main remark is that for $\theta_f = -\pi/2 \pm \pi$ the inductances are more affected by a significant decrease due to the local overflux concentration.

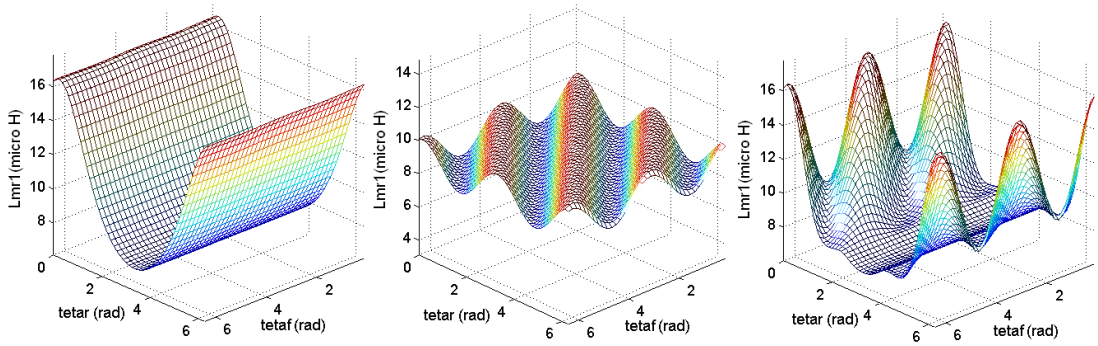

Fig. 8. First rotor loop magnetizing inductance L_{mr_1} in function of θ_r and θ_f for ($\delta_s = 0.4, K_s = 1$) (left), ($\delta_s = 0, K_s = 1.2$) (middle) and ($\delta_s = 0.4, K_s = 1.2$) (right).

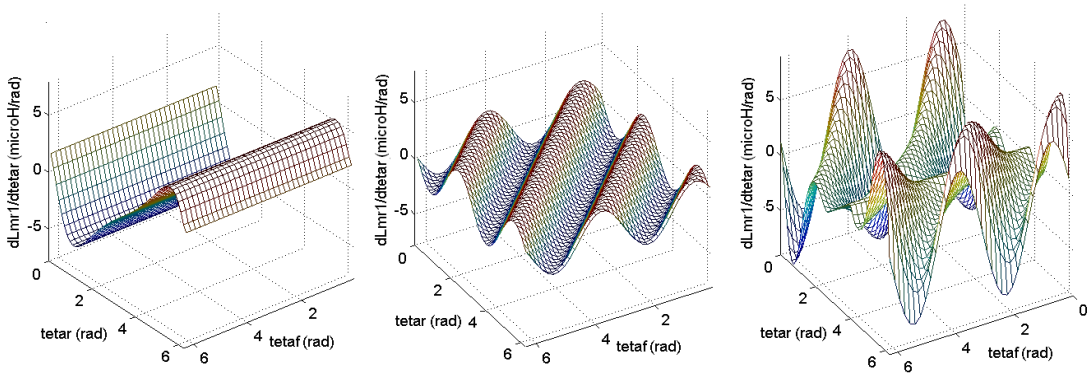

Fig. 9. First derivative of L_{mr_1} with respect to θ_r for ($\delta_s = 0.4, K_s = 1$) (left), ($\delta_s = 0, K_s = 1.2$) (middle) and ($\delta_s = 0.4, K_s = 1.2$) (right).

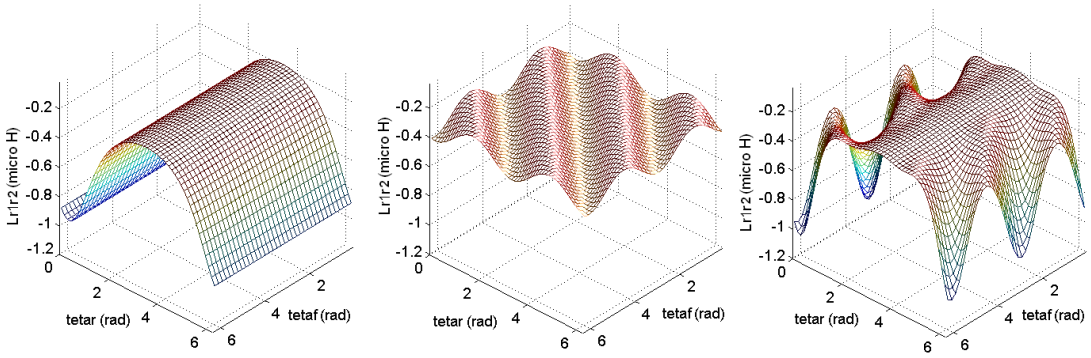

Fig. 10. Mutual inductance between the first rotor loops $L_{r_1 r_2}$ for ($\delta_s = 0.4, K_s = 1$) (left), ($\delta_s = 0, K_s = 1.2$) (middle) and ($\delta_s = 0.4, K_s = 1.2$) (right).

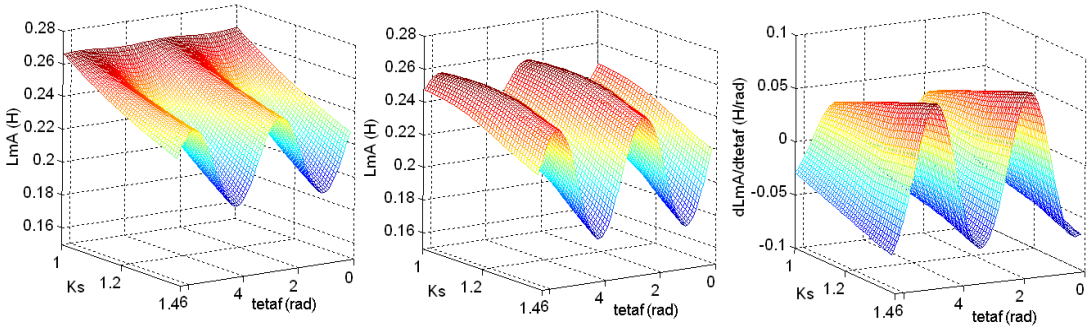

Fig. 11. Magnetizing inductance of stator phase A in function of K_s and θ_f in symmetrical condition (left) and that related to 40% of static eccentricity (middle) as well as its first derivative with respect to θ_f (right).

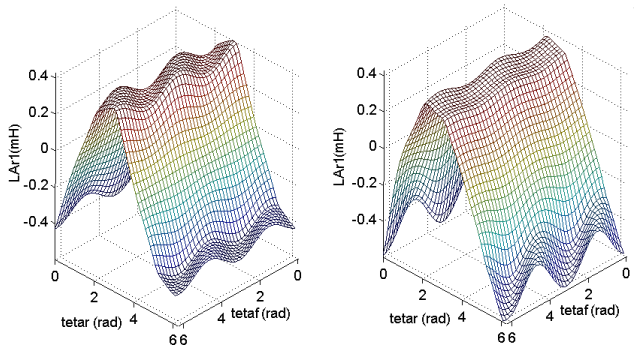

Fig. 12. Rotor-stator mutual inductance (L_{Ar_1}) in saturation condition in function of the rotor and field position ($K_s = 1.2$). Uniform air-gap (left) and 40% of static eccentricity (right).

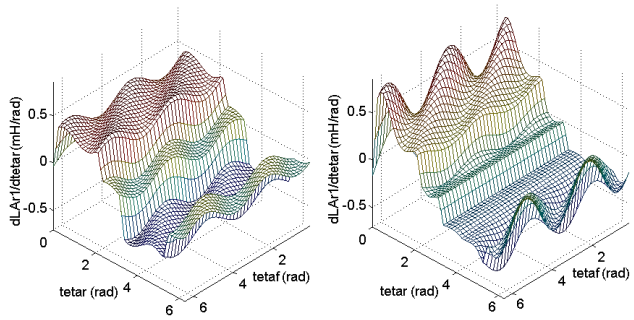

Fig. 13. First derivative of the rotor-stator mutual inductance (L_{Ar_1}) with respect to θ_r in saturation condition in function of the rotor and field positions ($K_s = 1.2$). Uniform air-gap (left) and 40% of static eccentricity (right).

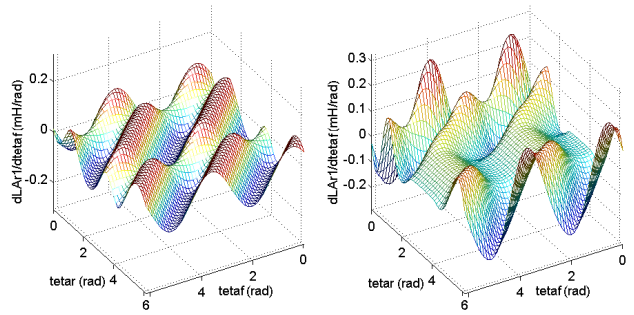

Fig. 14. First derivative of the rotor-stator mutual inductance (L_{Ar_1}) with respect to θ_f in saturation condition in function of the rotor and air-gap field positions ($K_s = 1.2$). Uniform air-gap (left) and 40% of static eccentricity (right).

IV. Conclusion

A new 2D-MWFA-based model of air-gap eccentricity in saturated IM was proposed to highlight the saturation effect on the flux density and the inductances. It considers a linear rise of the saturation factor along a particular region of the air-gap circumference. Saturation modeling in the air-gap eccentricity conditions can be done efficiently thanks to the described model which provides a full impedance calculation. Especially for a 2-pole motor, there is no concern as for the homopolar component arising from eccentricity [13]. Furthermore, we can consider the current as a state variable in an iterative resolution process of the IM circuital equations and then predict some of the motor behaviors via the current spectral content. The authors plan to complete this task in their future works.

V. References

[1] J. Faiz, B.M. Ibrahimi, H.A. Toliyat, "Effect of Magnetic Saturation on Static and Mixed Eccentricity Fault Diagnosis in Induction Motor," *IEEE Trans. Magn*, vol. 45, no. 8, pp. 3137-3144, Aug. 2009.

[2] X. Tu, L.A. Dessaint, R. Champagne, K. Al-Haddad, "Transient Modeling of Squirrel Cage Induction Machine Considering Air-gap Flux Saturation Harmonics," *IEEE Trans. Ind. Electr.*, vol. 55, no. 7, pp. 2798-2809, Jul. 2008.

[3] S. Nandi, "Modeling of induction machines including stator and rotor slot effects," *IEEE Trans. Ind. Appl.*, vol. 40, no. 4, pp. 1058-1065, Jul./Aug. 2004.

[4] H. A. Toliyat and T.A Lipo, "Transient analyze of induction machines under stator, rotor bar and end ring faults," *IEEE Trans. Energy Conv.*, vol. 10, no. 2, pp. 241-247, June 1995.

[5] T. Ilamparithi, S. Nandi, "Comparison of Results for Eccentric Cage Induction Motor Using Finite Element Method and Modified Winding Function Approach," *In Proc. of PEDES & 2010 Power India*, pp.1-7, Dec. 2010.

[6] S. Nandi, "A detailed model of induction machines with saturation extendable for fault analysis," *IEEE Trans. Ind. Appl.*, vol.40, no.5, pp. 1302-1309, Sept./Oct. 2005.

[7] J.C. Moreira, T.A. Lipo, "Modeling of saturated AC Machines Including Air-Gap Flux Harmonic Components," *IEEE Trans. Ind. Appl.*, vol. 28,no. 2, pp. 343-349, Mar./Apr. 1992.

[8] J. Faiz, M. Ojaghi, "Stator Inductance Fluctuation of Induction Motor as an Eccentricity Fault Index," *IEEE Trans. Magn*, vol. 47, no. 6, pp. 1775-1785, Jun 2011.

[9] M. Ossama, T.A. Lipo, "A New Induction Machine Model for Analysis of Eccentric Rotor Magnetic Pull," *In Proc. SPEEDAM*, vol. 1, pp. 173-177, June 1994.

[10] D.G. Dorrell, "Experimental behaviour of unbalanced magnetic pull in 3-phase induction motors with eccentric rotors and the relationship with tooth saturation," *IEEE Trans. Energ. Conv.,* vol. 14, no.3, pp. 304-309, Sept. 1999.

[11] A. Ghoggal, S.E. Zouzou, H. Razik, M.Sahraoui, A. Khezzar, "An improved model of induction motor for diagnosis purposes – Slot skewing effect and air-gap eccentricity faults," *Energ. Conv. Manag.* , vol.50, no. 2, pp. 1336-1347, 2009.

[12] A. Ghoggal, S.E. Zouzou, H. Razik, M. Sahraoui, A. Hadri-Hamida, "Application of the convolution theorem for the modeling of saturated induction motors," *In Proc. IEEE IECON'10*, USA, pp. 766-771, 2010.

[13] D. G. Donell, "Calculation of unbalanced magnetic pull in small cage induction motors with skewed rotors and dynamic rotor eccentricity", *IEEE Trans. Energ. Conv.,* vol. 11, no3, pp483-488, Sept. 1996.

VI. Biographies

Adel Ghoggal received the Electrical Engineer degree from the University of Biskra - Algeria in 1996. Between 1999 and 2003 he worked for the national company of electricity and gas (SONELGAZ) - Algeria. He received the "Magistère" degree in electrical engineering from the University of Batna in 2005 and the "Doctorat en sciences" degree from the University of Biskra in 2010. Dr. Ghoggal is an assistant professor with the University of Constantine Algeria since 2005 and a member of the "Laboratoire de Génie Electrique de Biskra" (LGEB) since 2007.

Salah Eddine Zouzou was born in Biskra, Algeria on 1963. He received the B.S degree from the "Ecole Nationale Polytechnique d'Alger", Algeria in 1987 and the M.S and Ph.D degrees from the "École Nationale Polytechnique de Grenoble" France in 1988 and 1991 respectively. His field of research interests deals with the design and condition monitoring; of electrical machines. He has authored or co-authored more than 40 scientific papers in national and international conferences and journals. Prof. Zouzou is an associate Professor at the University of Biskra, Algeria and he is the head of the LGEB since 2004.

Mohamed Sahraoui received the Engineer, the "Magistère" and the "Doctorat en sciences" degrees in electrical engineering from the University of Biskra, Algeria in 2001, 2003 and 2010 respectively. Dr. Sahraoui is an assistant professor with the University of Constantine, Algeria since 2005 and a member of the LGEB since 2007.

Hamid Derghal received the Engineer degree on electrical engineering from the University of Batna and the "Magistère" degree from the University of Biskra - Algeria in 1988 and 2000 respectively. Now, he is working toward the"Doctorat en sciences" degree on signal processing and faults detection. Mr Derghal is an assistant professor with the University of Biskra -Algeria and a member of the LGEB since 2004.

Amel Hadri-Hamida received the Engineer, the "Magistère" and the "Doctorat en sciences" degrees in electrical engineering from the University of Biskra, Algeria in 2002, 2005 and 2011 respectively. Dr. Hadri-Hamida is an assistant professor with the University of Constantine -Algeria and a member of the "Laboratoire d'Electrotechnique de Constantine" (LEC) since 2008.